Compound flood modelling framework for surface-subsurface water interactions

Francisco Peña[12345], Fernando Nardi[13], Assefa Melesse[4], Jayantha Obeysekera[5], Fabio Castelli[2], René M. Price[34], Todd Crowl[3], Noemi Gonzalez-Ramirez[6]

[1]WARREDOC, University for Foreigners of Perugia, Perugia, 06123, Italy
[2]Department of Civil and Environmental Engineering (DICEA), University of Florence, Florence, 50139, Italy
[3]Institute of Environment (InWE), Florida International University, Miami, FL, 33199, USA
[4]Department of Earth and Environment, Florida International University, Miami, FL, 33199, USA
[5]Sea Level Solutions Center, Florida International University, Miami, FL, 33181, USA
[6]Riada Engineering, Inc. P.O. Box 104, Nutrioso, AZ 85932, USA

Correspondence to: Francisco Peña (fpena023@fiu.edu)

Abstract. Compound floods are an active area of research where the complex interaction between pluvial, fluvial, coastal or groundwater flooding are analyzed. A number of studies have simulated the compound flooding impacts of precipitation, river discharge and storm surge variables with different numerical models and linking techniques. However, groundwater flooding is often neglected in flood risk assessments due to its sporadic frequency - as most regions have water tables sufficiently low that do not exacerbate flooding conditions -, isolated impacts and considerably less severity in respect to other types of flooding. This paper presents a physics-based, loosely-coupled modelling framework using FLO-2D and MODFLOW-2005 that is capable of simulating surface-subsurface water interactions. FLO-2D, responsible for the surface hydrology and infiltration processes, transfers the infiltration volume as recharge to MODFLOW-2005 until the soil absorption capacity is exceeded, while MODFLOW-2005 returns exchange flow to the surface when the groundwater heads are higher than the surface depth. Three events characterized by short-duration intense precipitation, average tide levels and unusually high water table levels are used to assess the relevance of groundwater flooding in the Arch Creek Basin, a locality in North Miami particularly prone to flooding conditions. Due to limitations in water level observations, the model was calibrated based on properties that have experienced repetitive flooding losses and validated using image-based volunteer geographic information (VGI). Results suggest that groundwater-induced flooding is localized, and high groundwater heads influence pluvial flooding, as the shallow water table undermines the soil infiltration capacity. Understanding groundwater flood risk is of particular interest to low-elevation coastal karst environments as the sudden emergence of the water table at ground surface can result in social disruption, adverse effects to essential services and damage of infrastructure. Further research should assess the exacerbated impacts of high tides and sea level rise on water tables under current and future climate projections.

1 Introduction

Flood inundation modelling is of critical importance for better planning, forecasting and decision-making practices (Teng et al., 2017). Scientific and technological innovations in numerical algorithms have continuously improved the performance of physically-based hydrologic, ocean circulation and hydraulic modelling packages to simulate faster and more accurate flood physical processes over the computational domain at various scales and resolutions (Devia et al., 2015). However, most flood inundation models are designed to simulate specific flood hazards (i.e., pluvial, fluvial, coastal, groundwater) independently and are unable to assess complex flood dynamics per se due to code limitations and burdensome compatibility. To address these numerical constraints, some models have the ability to operate as linked units or groups by using coupling schemes (i.e. one-way, loosely, tightly, fully) to build compound models capable of simulating multiple flood drivers (Santiago-Collazo et al., 2019).

Compound floods (CF) are high-impact low-probability events characterized by a non-linearity behavior resulted from the complex interactions of interrelated flood drivers triggered at the same spatial and temporal scales (Field et al., 2012; Seneviratne et al., 2012; van Westen and Greiving, 2017; Zscheischler et al., 2018). Research on CF has received increasing attention in recent years due to their adverse impacts at the global scale. Deterministic and probabilistic approaches are preferred frameworks to analyze CF events. Stochastic models through copula-based probability analysis and extreme value theory examine the interrelationship between flood drivers, while physically-based numerical simulations provide a tangible depiction of the flood dynamics for current and future climate projections. Several compound flooding studies have used physically-based hydrodynamic models as the reference model to simulate the combined effects of rainfall-runoff and storm surge (Christian et al., 2015; Gori et al., 2020; Ikeuchi et al., 2017; Karamouz et al., 2015; Kumbier et al., 2018; Olbert et al., 2017). Failure to consider the compound interactions of flood drivers can result in significant uncertainties in the magnitude, timing, and estimation of flood risk (Wahl et al., 2015). Therefore, the transition from traditional univariate approaches to a multivariate perspective is necessary to improve flood hazard understanding and predictions (Bates et al., 2021).

The significance of groundwater flooding is rarely disputed as it is only relevant to geographical regions sitting on top of permeable rock that are prone to groundwater emergence (i.e., Miami, Yucatán Peninsula, United Kingdom). Groundwater floods are events limited to prolonged rainfall in low-elevation karst watersheds characterized by unconfined aquifers that experience sudden increases of already high-water table levels above normal conditions (Finch et al. 2004). Although there has been a substantial increase in groundwater flooding literature since the 2000s as well as advances in understanding surface water/groundwater interactions (Brunner et al., 2017; Sophocleous, 2002), relevant knowledge gaps and lack of understanding of this phenomenon persist from the complex relationship between topography and hydrogeology (Bradford, 2002; Hughes et al., 2011; Ó Dochartaigh et al., 2019). The water table response time to hydrological events is controlled by the soil, vegetation and aquifer properties, which influence the infiltration capacity, recharge rate and response time (Nalesso, 2009). Similarly,

the groundwater dynamics are influenced by spatial-temporal variations of single or compound flood drivers (i.e. precipitation events, high river levels, above-average tides and sea level rise conditions) over long or repetitive periods of time (Ascott et al., 2017). Thus, the water table response to hydrological mechanisms (García-Gil et al., 2015), system fluctuations and residence time (MacDonald et al., 2014) determine the severity of groundwater flooding.

70

While probabilistic and empirical approaches have contributed to the development of regional groundwater flood maps (Cobby et al., 2009; Jacobs, 2007), physically-based models are scarce. Abboud et al. (2018) found that the June 2013 compound flood disaster in the Elbow River (Canada) was induced by steady precipitation and increased river flow discharges from upstream basins resulting in basement flooding due to the rise of the water table. The combined effects of fluvial and groundwater

75 flooding were not considered in that study since the MODFLOW river package focused exclusively on groundwater flow. Similarly, Yu et al. (2019) applied the coupled surface-subsurface model PIHM to produce a comprehensive groundwater flood risk and damage assessment over the Koiliaris River (Greece). Yang & Tsai (2020) investigated the impacts of water table dynamics on groundwater flooding and levee under seepage in New Orleans, Louisiana using MODFLOW-USG for hazard mapping, flood delineation and levee breach analysis. Su et al. (2020) developed a coupled model to assess the improved

80 response of the repaired storm drain system infrastructure with the shallow aquifer groundwater dynamics by coupling EPA SWMM with MODFLOW-2005 at the city of Hoboken in New Jersey (USA).

Previous efforts to model groundwater levels in South Florida have been developed in the form of hydrogeologic maps (Fish and Stewart, 1991), estimation of aquifer parameters to calculate groundwater flow (Cunningham et al., 2004), and statistical

85 analysis of hydrological measurements (Chebud and Melesse, 2012, 2011; Prinos and Dixon, 2016). Similarly, Hughes and White (2016) investigated the effect of pump practices and sea level rise on surface water routing and groundwater interactions in Miami-Dade County (MDC) using MODFLOW. Currently this is the main reference model for MDC regional research and planning purposes in hydrologic, ecologic, and environmental fields. Regarding the study area, Sukop et al. (2018) developed a MODFLOW model that analyzed the current and future response of the water table to rainfall events in a portion of the Arch

90 Creek Basin. The study highlighted precipitation as the main trigger for groundwater-induced flooding, with tidal fluctuations and sea level rise increasing the shallow water table. Researching the flood risk potential from surface-subsurface water interactions in MDC where the water table is near to the ground surface is critical as it could reveal hidden risks from the compound impact of major storms and coastal forcing variables for present and future scenarios.

95 The main purpose of this study is to present a loosely-coupled modeling framework capable of simulating surface and subsurface water interactions to advance flood vulnerability assessments in regions prone to groundwater-induced flooding and complex compound flooding phenomena. To better understand the effects of the water table in a low elevation coastal zone, a methodology is developed to couple the 2D hydrodynamic software FLO-2D and the groundwater model MODFLOW-2005. The Arch Creek Basin in North Miami was selected as an ideal test site due to its unique hydrogeomorphology, low-

100 lying topography, and high vulnerability to flood events. For the purpose of this analysis, three events characterized by short-lived heavy precipitation, regular tide levels and unusually high-water tables were selected to demonstrate the importance of simulating surface-subsurface water interactions in urbanized karst coasts, as high groundwater heads may exacerbate flooding conditions. In the context of this paper, compound flooding is defined as the interaction of overland flow and groundwater emergence, while surge levels are normal and have a minimal influence in the inundation beyond the coast. Finally, the coupled

105 model results were calibrated based on official database from FEMA and validated using volunteered geographic information (VGI) flood observations from the study area. The paper is organized as follows: a complete description of the study area is introduced (Section 2), followed by data collection and the methodology presented in Sections 3 and 4. Model calibration and results illustrate the main findings (Section 5); the discussion compares the results with similar work in the region (Section 6); and the conclusion section includes the advantages, limitations, and future research (Section 7).

110

2 Study Area

2.1 Site description

The Arch Creek Basin is located in the northeastern part of MDC, along the coast of Biscayne Bay in the city of North Miami, Florida. Prior to anthropogenic interventions, the Arch Creek River served as an important flow corridor that connected the

115 Everglades to Biscayne Bay, controlling the flood pulse dynamics in the tropical wetland system (Fig. 1).

The gradual modifications in land use and the construction of the Biscayne Canal in the 1920s marked the transition of the natural environment to agricultural lands. Variations in the soil moisture conditions and infiltration levels due to changes in the streamflow and drainage patterns in the area caused unsustainable farming practices that lead to a shift to residential

120 development (Fig. 2). The urbanization process along Biscayne Bay required considerable cut and fill earthworks to create ideal urban development conditions (Miami-Dade, 2016).

The Arch Creek Basin (16.95 km^2) is a low-lying coastal zone predominantly urbanized (90.1%) and economically diverse. The population is distributed within five jurisdictions, primarily concentrated in North Miami and North Miami Beach (Table

125 1). Although the topography is predominantly low and flat, some areas within the basin are considered the highest elevations in MDC ranging from 5 to 15 meters.

2.2 Climate

The climate of Miami and southeast Florida is characterized by wet (May to October) and dry seasons (November through April) with 75% of the annual rainfall occurring in the wet season (Abiy et al., 2019). The average annual rainfall is above

130 1500 mm and the average monthly precipitation during the wet season is above 150 mm (Abiy et al., 2019). Rainfall can vary

from year to year (1000 – 2000 mm/yr), due to tropical storms and extreme hydrometeorological events which highly influence rainfall amounts. A reported increasing trend in rainfall of 2.1 mm/yr from 1906 to 2016, mainly attributable to an increase in wet season rainfall (Abiy et al., 2019), underscores that MDC is under a continued threat from flooding.

2.3 Hydrogeology and groundwater

135 The Arch Creek Basin sits atop one of the most permeable aquifers in the world, known as the Biscayne Aquifer. The Biscayne Aquifer stores 34 billion m^3 of water and spans an area of 10,000 km^2 (Price et al., 2020) tapering from near the center of peninsula Florida towards the eastern coastline where its maximum thickness is about 38 meters (Parker and Cooke, 1944) and hydraulic conductivities exceeding 3,000 m/day (Fish and Stewart, 1991).

140 The stratigraphy of Biscayne aquifer consists entirely of unconfined permeable limestones of the Fort Thompson and Miami Limestone Formations and contains numerous solution conduits, resulting in rapid infiltration and recharge to the aquifer (Cunningham and Florea, 2009; Hoffmeister et al., 1967; Parker and Cooke, 1944). Recharge via precipitation occurs primarily in the Everglades and groundwater flows eastward towards the shore where it discharges to Biscayne Bay (Cunningham and Florea, 2009).

145 ## 2.4 Flood risk and vulnerability

Floods resulting from extreme weather and climate events represent a major threat to low-lying neighborhoods and housing infrastructure in the Arch Creek Basin. Historically, frontal systems and summer cloudbursts are responsible for most of the significant pluvial flooding events in the study area compared to strong tropical systems, with Hurricane Irene (1999), Katrina (2005), Irma (2017), and No-Name storms as the only exceptions (Miami-Dade, 2015).

150

Most of the population of MDC lives in high-risk areas, only 1.2 meters (4 feet) above sea-level. In regard to the Arch Creek Basin, three-quarters of the urban landscape (67%) are located in a 100-year flood-prone area, and over 80% of the housing stock was built prior the development of the 1973 Flood Insurance Rate Map (Miami-Dade, 2016). For instance, properties in the Arch Creek Estates and localized areas East of US-1 such as the Key Stone Islands and Sans Souci Estates experienced

155 repetitive flood losses since these settlements were built in the former riverbed of the Arch Creek Rivers or in land reclamation areas. The capacity of these communities to respond to hydrometeorological phenomena is limited or non-existent, resulting in repetitive negative impacts on livelihoods and residential property, expanding the socio-economic gap and inequality of MDC communities (Keenan et al., 2018).

160 Frameworks to integrate flood risk mitigation and climate change adaptation strategies are a main component in Miami Dade County's policy agenda (GM&B, 2019). As a result, the Arch Creek Basin received the designated status of "Adaptation Action Area", the first pilot project in Florida to build social, environmental and economic resilience (Miami-Dade, 2016).

3 Data description

165 This section presents the data sets required to build the 2D surface-subsurface flood modelling study, including the topographic input, and hydrologic monitoring stations that provide rainfall, tide and well gauge records, as well as verified flood observations.

3.1 Topography

The Light Detection and Ranging (LiDAR) digital elevation model (DEM) is a 2-meter spatial resolution produced by Miami-
170 Dade County, Florida. The LiDAR scanner corresponds to the actual bare-earth surface, removing tops of vegetation, buildings, and vehicles, and the project coordinate system is UTM zone 17N Horizontal Datum WGS84. In terms of elevation, the North American Vertical Datum of 1988 (NAVD 88) was assigned as the reference geodetic vertical datum for this study, substituting the original measurements based on the National Geodetic Vertical Datum of 1929 (NGVD 29).

3.2 Hydrologic input

175 Hydrologic modeling included hydrologic conditions of the time periods 1-4 October 2000, 6-8 June 2013, and 23-26 May 2020. Boundary and initial hydrologic inputs such as precipitation, tide and ocean-side water levels, and groundwater heads over the specified time periods were obtained from the following sources.

3.2.1 Rainfall

The NEXRAD Radar Rainfall Application is a scientific web map interface developed by the South Florida Water Management
180 District (SFWMD) on which rainfall data is reported based on spatial coverage configurations in the form of the entire district, counties, Arch Hydro Enhanced Database (AHED) watersheds, or Rain Grid. The NEXRAD Rain Grid Layer is a 2 km grid resolution that provides an accurate representation of precipitation every 15 minutes. Rainfall Grid cell 10044042 was selected to characterize the Arch Creek Basin's rainfall conditions.

3.2.2 Tides and ocean-side water levels

185 DBHYDRO is the official SFWMD repository for climate, hydrologic, and environmental databases (https://www.sfwmd.gov/science-data/dbhydro). Ocean-side water levels were obtained from stations S28_H and S28_T, located in the Biscayne Canal Number C-8 on the Arch Creek southern boundary edge.

The NOAA Tides & Currents website (https://tidesandcurrents.noaa.gov/) provides local water levels, tides, current predictions, and other oceanographic and meteorological conditions. The closest coastal sensor to the Arch Creek Basin is
190 located at the Virginia Key, Biscayne Bay Station (ID #8723214).

3.2.3 Groundwater heads

The Unites States Geological Survey (USGS) National Water Information System (https://waterdata.usgs.gov/nwis/gw), in cooperation with the SFWMD, records daily summary data of maximum groundwater levels in the south Florida region. The groundwater level data was obtained from well G-852 adjacent to the outer western boundary of the study area (Fig. 3). Daily field water level measurements have been recorded since 1973, and 15-minute intervals since October 2007.

3.3 Repetitive flood claims

FEMA's severe repetitive loss properties program is designed to provide grants and financial assistance to residential properties that have experienced frequent flood losses over the years (FEMA, 2021). Currently, seventy-five properties have requested financial assistance for property acquisition or to recoup with some of their investments due to flood damages in the Arch Creek Basin (Miami-Dade, 2017). The database stores detailed information on the date of loss, building type, flood zone designation, type of insurance and claim payments between 1995 to 2015, providing a clear footprint of flooding risk hotspots and flood prone communities. This dataset will be used to calibrate the flood inundation maps.

4 Methodology

4.1 Hydraulic Model: FLO-2D

FLO-2D is a physically-based volume conservation model that combines hydrology and hydraulics to simulate the propagation of water dynamics in urban, riverine, and coastal environments for flood hazard mapping, floodplain delineation, flood vulnerability assessments and mitigation planning (O'Brien et al., 1993). The flood routing model applies the dynamic wave approximation to the momentum equation to calculate the average flow velocity across the square grid system one direction at a time in eight potential flow directions over the floodplain. Hydrological processes are represented as rainfall data over the computational domain or as input hydrographs that can be specified in the channel, floodplain, or along the coasts. Various attributes (elevations, roughness coefficient), components (channel, infiltration, storm drain) and features (streets, hydraulic structures) can be incorporated into the FLO-2D model to produce more refined simulations (O'Brien, 2011). Details are described elsewhere (Annis and Nardi, 2019; Grimaldi et al., 2013; Peña et al., 2021; Peña and Nardi, 2018).

4.2 MODFLOW-2005

MODFLOW-2005 is a fully distributed model developed by the USGS that simulates groundwater flow in aquifer layers (confined or unconfined) using a block-centered finite-difference approach (Harbaugh, 2005). The spatial discretization of the aquifer(s) into grid elements computes the horizontal and vertical flow stresses of the hydrogeological system (water heads, recharge, zetas) at the center of the cell. Similarly, the model offers several solvers for matrix equations, as well as subsidence, observations, surface-water routing, and transport packages. Technical documentation on the model description and groundwater flow equations is presented in Harbaugh (2005).

4.3 Coupling surface-groundwater models

The main factors determining the coupling process between FLO-2D and MODFLOW-2005 include the algorithms' mathematical solver compatibility to calculate and transfer the exchanged volumes in opposite directions within a fully integrated framework and share consistent spatial and temporal scales.

In terms of the spatial scale, a perfect match between FLO-2D and MODFLOW-2005 surface elevation layers is necessary for the surface and subsurface water interactions to happen. This agreement is subject to identical geographical position, reference system, size resolution, and topographic cell elevations (Fig. 4). Although the coupled models can have variations in the number of cells and domains, FLO-2D cells must overlap the MODFLOW-2005 grid domain system to compute results and transfer the output data from one model to another and vice versa until the end of the simulation.

A significant advantage in the coupling process is that both numerical codes are written in FORTRAN programming language and shared the same explicit finite difference method simulating all physical processes simultaneously in a fully integrated framework. Nevertheless, FLO-2D and MODFLOW-2005 design structures present significant operability differences to perform calculations. Both numerical algorithms solve the two- and three-dimensional equations independent from each other to satisfy their respective numerical stability criteria and accuracy. For this reason, a loosely-coupled linking technique in order for FLO-2D and MODFLOW-2005 to exchange output in a synchronized systematic way and simulate the surface-subsurface interactions within the same modelling framework. In MODFLOW-2005, the simulation is divided into a series of stress periods within which specified data are constant. Each stress period, in turn, is divided into a series of time steps. The solution of the finite difference equations can be written in matrix form as:

$$[A]\{h\} = \{q\} \tag{5}$$

where $[A]$ is a matrix of the coefficients of the head for all active nodes in the grid, $\{h\}$ is a vector of head values at the end of time step n for all grid nodes, and $\{q\}$ is a vector of the constant heads for each timestep.

250

MODFLOW-2005 has three internal nested loops, the stress period loop (outer), time step loop (intermediate), and iteration loop (inner). A predetermined procedure is implemented at the beginning as a routine setup function to read the domain set-up (i.e., grid resolution, number of layers, and simulation time), model data in the form of boundary conditions, aquifer hydraulic characteristics (i.e., hydraulic conductivity, specific storage, transmissivity), initial head conditions, and selected
255   solution method.

The outer loop is responsible for calculating the resulted heads for each timestep from defined boundary conditions, including specified heads (i.e., time-variant or head boundary packages), specified flux (i.e., recharge or wells), and head-dependent flux (i.e., drain, evapotranspiration or river recharge). The intermediate loop accounts for the total simulation time, as well as
260   additional output processing, and the inner loop for calculation purposes to approximate the head solution until the maximum number of iterations is achieved. At the end of the iteration loop, specified output control files are created in the form of heads, budget terms, or flow in the domain. The intermediate and outer loops repeat until all timesteps are completed for all stress periods (Harbaugh, 2005).

265   FLO-2D works with variable time steps that are automatically adjusted internally based on stability criteria requirements. Because FLO-2D uses an explicit finite difference method to solve the surface water equations, its time step is usually much smaller than that defined for the MODFLOW-2005 model, resulting in an increasing number of 2D computational sweeps to match the MODFLOW-2005 simulation time (FLO-2D, 2018). A time-synchronization scheme was developed to achieve the coupling, as the MODFLOW-2005 intermediate loop is in charge of transferring the information between models. For example,
270   the FLO-2D iterative calculations start until reaching MODFLOW-2005 time step one. Then, the MODFLOW-2005 intermediate loop performs its respective calculations from time step one and is shared in both directions to continue with the following time step (Nalesso, 2009). The process repeats itself until the simulation time of FLO-2D is completed. Similarly, MODFLOW-2005 can experience numerous stress periods during the simulation. Fig. 5 depicts the time step synchronization procedure between both models.

275

The Green & Ampt method (1911) was selected for being the most complete function available in FLO-2D that calculates the accumulated volume of water that infiltrates from the surface layer into the soil and is transferred to MODFLOW-2005 as recharge. The unsaturated zone is not considered in the coupling methodology as the infiltrated volume travels directly to the water table. Rainfall intensity predominantly influences the infiltration process as runoff and is generated when the maximum
280   infiltration capacity is exceeded. Several variables are accounted for in the Green & Ampt infiltration function, including initial abstraction, hydraulic conductivity, soil porosity, volumetric moisture deficiency (initial and final soil saturation conditions),

soil suction and soil storage depth. The development of the Green & Ampt method in FLO-2D is based on the application of Darcy's Law principle that the infiltration process begins as soon as the surface water moves in a vertical direction through the permeable medium and can be written as:

285

$$\frac{\Delta F}{\gamma} - ln\left(1 + \frac{\Delta F}{\gamma + F(t)}\right) = \frac{K_w}{\gamma} \Delta t \qquad (6)$$

Where:

ΔF = change in infiltration over the computational time step
290 K_w = hydraulic conductivity at natural saturation (mm/hr)
$\gamma = (PSIF + Head) * DTHETA$
$PSIF$ = capillary suction (mm)
$Head$ = incremental rainfall for the time step plus flow depth on the grid element (mm)
$DTHETA$ = volumetric soil moisture deficit (dimensionless)
295 $F(t)$ = total infiltration at time t
Δt = computational time step

Fullerton (1983) developed an explicit equation ΔF by using a power series expansion for infiltration with respect of time to approximate the logarithmic term in the latter equation:

300

$$\Delta F = \frac{-[2F(t) - K_w\Delta t] + [(2F(t) - K_w\Delta t)^2 + 8K_w\Delta t(\gamma + F(t))]^2}{2} \qquad (7)$$

Fig. 6 provides a schematic representation of how the simulated groundwater heads of MODFLOW-2005 are incorporated in the infiltration methodology of FLO-2D. The infiltration methodology was developed under the principle of hydrostatic
305 pressure and the assumption that the piezometric head is similar to the datum elevation in unconfined aquifers (Nalesso, 2009). The soil saturation percentage is determined based on the surface flow and water table levels. The infiltration calculation continues as long as the water table levels are lower than the terrain elevation. Conversely, the water exchange can also occur in the opposite direction due to a sudden rise in the water table. If the groundwater heads calculated in MODFLOW-2005 are higher than the surface depth in FLO-2D, the depth of water from groundwater will be added to the surface depth. The
310 infiltration calculation is switched off at each node as long as the saturation condition persists, meaning that infiltration will not be calculated until the soil absorption capacity is reestablished.

4.4 Model configuration and set-up

The FLO-2D hydraulic model requires a grid of square cells to represent the topography of the floodplain domain. The
315 structured grid size of the computational domain defines the hydraulic model resolution. The LIDAR DTM was used as source floodplain topographic information, and an interpolation algorithm was implemented to produce a resampled DTM floodplain

model to be used as input elevation of the hydraulic model. The nearest neighbor interpolation method was selected to resample data from the high-resolution 2 m LiDAR to a 20m resolution (42,621 cells).

320 In addition to the topographic features, a detailed representation of the built environment is relevant for urban flood modeling in order to simulate the flow wave propagation dynamics realistically. All buildings in the domain (7827 features) were imported to the FLO-2D computational domain. The polygon vectors are represented as Area Reduction Factors (ARF = 1) where the grid element surface area is considered impervious and is removed from potential water interactions.

325 Rainfall and tides were considered for the hydrologic forcing, setting the precipitation over the grid system and tide levels in the easternmost cells to represent the Biscayne Bay's coastal conditions. Both time series are structured on a one-hour basis and are presented in the following section. The inclusion of the storm drain system, French drains, surface water control structures and pump stations in the modelling framework is beyond the scope of this study.

330 The infiltration method selected for the case study was the Green & Ampt. Global soil parameters correspond to the urbanized and permeable surfaces characteristics. Considering that MDC is characterized by the water table response to rainfall events, conservative infiltration estimates for the impermeable surfaces were selected to account for the influence of the French drains in the system. For simplicity, the Manning roughness coefficient was assumed as 0.40 for green land cover areas and 0.04 for the impervious urbanized environment, canal bed, and Biscayne coast.

335
Bathymetric measures were available for the Little Arch Creek River. A 1D hydraulic model with natural cross-sections was imported into FLO-2D extending from NE 143rd Street to structure G-58 located downstream of the Enchanted Forest Elaine Gordon Park. Official bathymetry from the Biscayne shore, Keystone Island, and Sans Souci canals was not available for this study due to jurisdiction restrictions. To compensate for the missing geometry, aerial imagery Google Earth was used to

340 measure the canal's width, while a 10-meter bottom elevation was used as constant depth based on the Miami Florida Intracoastal Topography database from the Oleta River.

Concerning MODFLOW-2005, a simple model was developed based on the regional groundwater model of MDC developed by USGS (Hughes & White, 2016) using an advanced version of MODFLOW-2005 that applies the Newton-Raphson

345 formulation (MODFLOW-NWT) with the Surface-Water Routing (SWR1) Process to simulate comprehensive surface and groundwater hydrologic conditions on a 15 meter grid resolution; the second model consists of a local 1D MODFLOW that simulates the influence of the water table on flooding conditions in an upper portion of the Arch Creek Basin (Sukop et al., 2018).

350 The boundary area applicable to the Arch Creek Basin was extracted from the regional model using the ModelMuse graphical user interface (Winston, 2009), and the grid spacing across the model was regenerated to a 20 meters resolution. The spatial discretization of the model on the horizontal axis consists of 265 columns and 285 rows for a total of 75,525 cells. The Biscayne aquifer is simplified to be a one-layer 35 meters thickness compared to the three layer units of the regional hydrogeological system. Taking the upper aquifer parameters as reference, the hydraulic conductivities (Kx≈1,890 meter/day), specific storage

355 (Ss = 1.27 e^{-5}) and specific yield (Sy≈ 0.376) vary across the domain. Four boundary conditions are assigned in respect to the hydrological forcing in the study area. The Time-Variant Specified-Head (CHD) package feature in the easternmost boundary represents the tide conditions of the Biscayne Bay and the ocean-side water levels from Canal C-8 in the southern boundary edge. In respect to the groundwater heads, the General-Head Boundary (GHB) package was used to set the water table levels from gauge station G-852 in the westernmost boundary of the domain. MODFLOW-2005 package solvers were customize

360 based on the local groundwater model. The stress periods are structured in one-hour to match the FLO-2D time steps, and the groundwater flow calculations are under transient state.

After the modelling set-up, the compatibility process validates the perfect agreement between the surface layers of FLO-2D

365 and MODFLOW-2005 in order for the loosely-coupled model to link the floodplain-aquifer hydrodynamics. If so, FLO-2D will act as the base hydraulic model responsible for simulating precipitation and ocean levels with the support of MODFLOW-2005 to simulate the groundwater heads, creating a compound flood modelling framework for surface-subsurface water interactions (Fig. 7).

370 **4.5 Flood events**

Three flood events characterized by similar high intensity rainfall, tide levels, and unusually high-water table levels with different response times were selected to compare the surface-subsurface model results (Fig. 8). Tropical Storm Leslie (2-4 October 2000) was responsible for one of the most severe events of North Miami in recent history in terms of flooding and property damages, with an accumulated rainfall of 454 mm over 65 hours and an estimated return period of 50 years (Franklin

375 et al., 2001). Similarly, Tropical Storm Andrea (6-8 June 2013) was a short-lived storm that formed in the Gulf of Mexico which produced very heavy precipitation across Broward and MDC (Beven II, 2013), and a total rainfall of 317 mm in the Arch Creek Basin. The 25 May 2020 event is categorized as a 25-year storm with a total daily rainfall depth of 263 mm, producing localized rainfall in the North Biscayne Bay watershed, specifically in the Arch Creek Basin, due to antecedent rainfall conditions since mid-April 2020.

380

5 Results

5.1 Calibrated coupled surface-subsurface model

Simulating surface-subsurface water physical processes through physics-based flood modelling frameworks is relevant and meaningful to better assess the severity of groundwater-induced flooding in low elevation coastal environments characterized by porous permeable soil. Fig. 9 illustrates the simulated maximum inundation depths corresponding to the magnitudes of Tropical Storm Leslie, Tropical Storm Andrea, and the 25 May 2020 storm. Tide levels per se do not pose significant threats to infrastructure as the coastal waters remain within the channels. Fig. 10 illustrates the emergence of the groundwater heads to the surface as a result of the increase in the water table. The simulation proves reasonable in terms of maximum flood depth and extent due to the similarities in the hydrologic conditions, being Tropical Storm Leslie the most severe of all three storms. FEMA's records on properties subject to frequent flooding were used as a calibration approach to verify a match between the model results with flood observations. Although the available records do not specify the observed inundation depths, an agreement between the property locations and maximum water levels may offer sufficient evidence that the model provides reasonable results (Fig. 11). The calibrated results and display of the water table timeseries in selected locations for Tropical Storm Leslie are shown in Fig. 12-13.

5.2 Identification of flooding hotspots

The groundwater flood maps for Tropical Storm Leslie (37.17%), Tropical Storm Andrea (13.87%) and the May 2020 event (20.82%) are showed in Fig. 10. The simulation demonstrates that slight variations in the water table depth (Fig. 8) can exacerbate groundwater emergence extent, resulting in ≈ 10 cm across the Arch Creek Basin. Interestingly heavy precipitations scenarios with very high water tables over extended periods of time (May 2020 event) are more likely to trigger groundwater induced flooding compared to very high precipitation with high water table levels (Tropical Storm Andrea). Fig. 11 presents reasonable results between the reported claims and localized flooding, indicating that the housing infrastructure in these neighborhoods are likely to experience additional flood losses at some point in the future. The simulated storm events illustrate that most of the properties experienced moderate to high flood depths (> 0.5 meters) in predefined locations. Although rainfall-runoff is the primary source of flooding in the urbanized Arch Creek Basin, abnormally high groundwater levels triggered groundwater-induced flooding near historic waterways and zones below the County's land elevation flood criteria, with flood depths ≈ 1 meter (Fig. 12a – 12b). The groundwater plots illustrate the effect of tidal and groundwater boundary conditions on the behavior of the simulated water table, in turn demonstrating the importance of both variables in the modeling set-up and influence in subsurface dynamics, as a cyclic high-low pattern characterizes the tide fluctuations of the Biscayne Bay (Fig. 12b – 12e) compared to the defined water heads behavior from well G-852 in the western boundary of the domain (Fig. 12a, 12f). In terms of residential damage, Tropical Storm Leslie and Tropical Storm Andrea may be considered the costliest events in the Arch Creek Basin as both account for 60% of the reported claims (25 and 17 respectively) (Table 2).

415 Sources of uncertainty in the coupled numerical model could be reduced by increasing the model's resolution and incorporating storm-water infrastructure features (i.e., French drains). For example, the increase of the water table levels could challenge the ability of the storm drain system to convey water towards the Bay, resulting in prolonged flooding conditions, or anti-flood pump stations may alleviate the impacts of flooding by draining water from the streets and swales back to the ocean. Nevertheless, the repetitive loss records only reflect a small percentage of the damaged infrastructure and cannot be generalized

420 at the Basin scale as the property owners may not meet the criteria to file the claim. Therefore, the presented modelling results fall more on the conservative side and might overestimate the real flooding conditions.

5.3 Validation using crowdsourced data from Tropical Storm Andrea

A limited number of real-time crowdsourced flooding observations in the Arch Creek Basin were available for Tropical Storm

425 Andrea (Fig. 13). The visual comparison indicates a spatial agreement between the maximum flood depth of the coupled simulation and the interpreted depth of the crowdsourced data (Table 3). Fig. 12a associates high flow depths (> 0.5 meters) with several properties that have experienced regular flooding conditions, while the crowdsourced photograph displays an estimated inundation depth of 0.20 meters. Despite the model's overestimation, this comparison can be seen as an effective form of validation considering the changes in land use associated with the Arch Creek flow (Fig. 2) and low topographic

430 elevation (Fig. 3b). Regarding Fig. 13b, the US Post Office exhibits chronic flooding in the parking lot. The coupled model exhibits a reasonable level of accuracy in terms of flood depth validation results. Fig. 13c displays stagnant flood water accumulated post-event in a portion of the NE 14 Ave. The results suggest that the rise of the water table do not influence the inundation depth and extents in any of these locations. Despite the limitations on the amount of collected crowdsourced data in the study area, a larger georeferenced dataset including the date and time could improve the reliability of VGI data to validate

435 hydrodynamic models.

6 Discussion

The results of this investigation determined that areas in the Arch Creek Basin below 1.0 meter elevation are potentially

440 vulnerable to groundwater-induced flooding (Fig 10, 12a, 12b). Similar results were obtained by Sukop et al. (2018) who found that precipitation as the main trigger for rainfall-induced and groundwater-induced flooding in elevations below 0.9 meters and 1.5 meters respectively, with tidal fluctuations and sea level rise increasing the shallow water table, contributing to the reduction of the storm drain capacity. The present study also determined that antecedent rainfall events were important in the height of the water table at the start of the rainfall events investigated.

445

A simple groundwater model was approximated to be 2D in the horizontal axis and 1D in the vertical axis. Considering that most of the water table interactions occurred in the upper aquifer layer of the regional model (≈ 7 meters) and the short simulation time of the selected events (64 and 84 hours), we presume that differences in the modelling set up are not significant compared to the regional model and can be considered adequate for the purpose of this study. Additional work may be

450   necessary for the coupled model to be fully operational as the groundwater model should represent the heterogeneous aquifer system to assess the sensitivity of the water table dynamics.

Seasonal water table fluctuations are expected throughout the year, presenting a higher level frequency during the winter and spring seasons due to climate variability and hydrological forcing (Gurdak et al., 2009; Taylor and Alley, 2001). Nevertheless,

455   as we observed with Tropical Storm Leslie and Tropical Storm Andrea, the potential rise of groundwater levels to the surface during dry season cannot be ruled out since the hydraulically non-restrictive nature of the carbonate strata in MDC allows for rapid infiltration and high recharge rates during heavy precipitation events. The hydrologic forcing input and modeling results suggest that the joint occurrence of a high-intensity short-duration precipitation (> 50 mm peak, 250 mm total) with already high groundwater levels (> 1 meter) result in a CF event. Further research on linking multivariate statistical analysis with

460   coupled hydrodynamic modeling frameworks may prove beneficial to identify thresholds that trigger CF conditions (Couasnon et al., 2018; Jane et al., 2020; Moftakhari et al., 2019; Saksena et al., 2019; Sebastian et al., 2017; Serafin et al., 2019).

Although this investigation determined that rainfall and tide levels alone did not produce significant flooding, the modeling efforts did not include storm surge flooding that are often accompany by large hurricanes (Zhang et al., 2013). Nonetheless

465   induced storm surge flooding conditions and sea level rise projections are beyond the scope of this study, future work on assessing the impact of high tide and storm surge induced flooding are fundamental to assess CF events and future flood risk scenarios (Obeysekera et al., 2019).

7 Conclusions

Surface-subsurface water interactions are increasing in coastal cities due to multiple factors related to climate change. The Arch Creek Basin in North Miami, which served as a vital flow corridor that connected the Everglades to the Biscayne Bay, is an appropriate location to study the influence of high water tables in flood conditions. Results corroborate that groundwater-induced flooding is localized; thus, becoming an underlying condition that must be considered in low elevation coastal karst environments where the water table dynamics are subject to swift fluctuations caused by rainfall events.

A knowledge gap regarding a consolidated groundwater modelling framework was identified and addressed by proposing a loosely-coupled flood model that integrates surface hydrology and groundwater. The ability to produce more comprehensive flood hazard mapping from coupled surface and subsurface water interactions is scientifically relevant to professionals in hydroinformatics since it improves the replicability of flood dynamics, setting the path to improve the understanding, prediction, and response time of groundwater levels as a potential trigger to compound flooding phenomena that can exacerbate floodwater depth and areal extent. This work opens new horizons on the development of CF models from a holistic perspective.

The quality and accuracy of flood hazard mapping in urban areas are strictly related to the model spatial resolution considering that the vertical datum and built-up environment influence flow propagation dynamics. A 20-meters grid resolution was selected to balance the computational demands with a certain level of precision without compromising the quality of the simulation. However, the investigation of higher and coarser resolutions in surface-subsurface modelling studies might yield insights into the estimation of inundated areas and time performance at different scales.

Considering Miami's hydrogeomorphology is one of the most complex globally, the compounding effects of flood drivers may respond differently in diverse geographic settings. Therefore, further research should consider the proposed modeling framework to assess the CF risk in different geographical regions prone to multiple flood drivers, specifically in areas that have access to post-event flooding maps in the form of remote sensing products or VGI data for calibration and validation purposes.

The contributions of this research are substantial and go beyond the numerical simulation scope, as it supports numerous fields and real applications including flood management, urban planning and design, flood mapping and zoning, disaster risk reduction, flood insurance policies and policy making. The ability to simulate rising groundwater levels may be of great interest to Miami-Dade authorities on the impact of flooded septic systems and pollutants from a water quality, ecological and public health perspective. Ultimately, this research is a small piece of multidisciplinary work that analyzes the ripple effects of flooding in a wide range of fields (such as socio-economic costs, urban and ecological degradation, and health) and can set the basis for prevention, protection, accommodation, and even retreat/relocation policies.

Author contributions.

505 FP and JO jointly conceptualized the research experiment, from the design of the procedure to the presentation of results. FP gathered and processed the case study data, developed the coupled model framework, calibrated, and validated the simulation results, wrote initial version of manuscript, and produced all figures and tables. NGR provided the technical expertise to achieve the coupling between FLO-2D and MODFLOW-2005. FN, JO, and AM provided guidance and supervised the work of FP. RP and FC shared ideas to improve the results and discussion sections. FN, AM, JO, RP, FC, and TC contributed to the

510 paper revisions.

Competing interests. The authors declare that they have no conflict of interest.

Acknowledgements. We gratefully acknowledge Marcia Steelman from MDC for the kind support throughout this research,

515 including the provision of detailed background of the study area, documentation, historic imagery, shapefiles, and crowdsourced data. We thank Angela Montoya from MDC for her helpful assistance on understanding MDC's regional groundwater model using MODFLOW, and Ruben Arteaga from SFWMD for sharing flood protection and planning drainage reports. We would also like to thank our colleagues Michael C. Sukop and Martina Rogers from FIU for their valuable tutoring and recommendations during the development phase of the Arch Creek MODFLOW model.

520

Financial support. This work was supported by the University for Foreigners of Perugia— ISPRA INFO/RAC2020 Research Grant No. COAN AC.11.04.01 (Research grant "Research and implementation of GIS and hydrologic-hydraulic models for large scale water and flood risk management to support the Disaster Risk Reduction program"). In addition, this material is based upon work supported by the National Science Foundation under Grant No. HRD-1547798. This NSF Grant was awarded

525 to Florida International University as part of the Centers for Research Excellence in Science and Technology (CREST) Program. This is contribution number 1037 from the Southeast Environmental Research Center in the Institute of Environment at Florida International University. This work was also funded by Florida International University Sea Level Solution Center Grant No. 800008174, and the Dissertation Year Fellowship from the FIU University Graduate School.

References

Abboud, J.M., Ryan, M.C., Osborn, G.D., 2018. Groundwater flooding in a river-connected alluvial aquifer. J. Flood Risk Manag. 11, 1–11. https://doi.org/10.1111/jfr3.12334

Abiy, A.Z., Melesse, A.M., Abtew, W., Whitman, D., 2019. Rainfall trend and variability in Southeast Florida: Implications for freshwater availability in the Everglades. PLoS One 14, 1–20. https://doi.org/10.1371/journal.pone.0212008

Annis, A., Nardi, F., 2019. Integrating VGI and 2D hydraulic models into a data assimilation framework for real time flood forecasting and mapping. Geo-Spatial Inf. Sci. 22, 223–236. https://doi.org/10.1080/10095020.2019.1626135

Ascott, M.J., Marchant, B.P., Macdonald, D., McKenzie, A.A., Bloomfield, J.P., 2017. Improved understanding of spatio-temporal controls on regional scale groundwater flooding using hydrograph analysis and impulse response functions. Hydrol. Process. 31, 4586–4599. https://doi.org/10.1002/hyp.11380

Bates, P.D., Quinn, N., Sampson, C., Smith, A., Wing, O., Sosa, J., Savage, J., Olcese, G., Neal, J., Schumann, G., Giustarini, L., Coxon, G., Porter, J.R., Amodeo, M.F., Chu, Z., Lewis-Gruss, S., Freeman, N.B., Houser, T., Delgado, M., Hamidi, A., Bolliger, I., McCusker, K., Emanuel, K., Ferreira, C.M., Khalid, A., Haigh, I.D., Couasnon, A., Kopp, R., Hsiang, S., Krajewski, W.F., 2021. Combined Modeling of US Fluvial, Pluvial, and Coastal Flood Hazard Under Current and Future Climates. Water Resour. Res. 57, 1–29. https://doi.org/10.1029/2020wr028673

Beven II, J.L., 2013. Tropical Storm Andrea (AL012013). Miami FL.

Bradford, R.B., 2002. Volume-duration growth curves for flood estimation in permeable catchments. Hydrol. Earth Syst. Sci. 6, 939–947. https://doi.org/10.5194/hess-6-939-2002

Brunner, P., Therrien, R., Renard, P., Simmons, C.T., Franssen, H.J.H., 2017. Advances in understanding river-groundwater interactions. Rev. Geophys. 55, 818–854. https://doi.org/10.1002/2017RG000556

Chebud, Y., Melesse, A., 2012. Spatiotemporal Surface-Groundwater Interaction Simulation in South Florida. Water Resour. Manag. 26, 4449–4466. https://doi.org/10.1007/s11269-012-0156-4

Chebud, Y., Melesse, A., 2011. Operational Prediction of Groundwater Fluctuation in South Florida using Sequence Based Markovian Stochastic Model. Water Resour. Manag. 25, 2279–2294. https://doi.org/10.1007/s11269-011-9808-z

Christian, J., Fang, Z., Torres, J., Deitz, R., Bedient, P., 2015. Modeling the Hydraulic Effectiveness of a Proposed Storm Surge Barrier System for the Houston Ship Channel during Hurricane Events. Nat. Hazards Rev. 16, 04014015. https://doi.org/10.1061/(asce)nh.1527-6996.0000150

Cobby, D., Morris, S., Parkes, A., Robinson, V., 2009. Groundwater flood risk management: Advances towards meeting the requirements of the EU floods directive. J. Flood Risk Manag. 2, 111–119. https://doi.org/10.1111/j.1753-318X.2009.01025.x

Couasnon, A., Sebastian, A., Morales-Nápoles, O., 2018. A Copula-based bayesian network for modeling compound flood hazard from riverine and coastal interactions at the catchment scale: An application to the houston ship channel, Texas. Water (Switzerland) 10. https://doi.org/10.3390/w10091190

Cunningham, K.J., Carlson, J.L., Wingard, G.L., Robinson, E., Wacker, M.A., 2004. Characterization of aquifer heterogeneity

using cyclostratigraphy and geophysical methods in the upper part of the Karstic Biscayne Aquifer, Southeastern Florida, Water-Resources Investigations Report. https://doi.org/10.3133/wri034208

Cunningham, K.J., Florea, L.J., 2009. The Biscayne Aquifer of Southeastern Florida The Biscayne Aquifer of Southeastern Florida 196–199.

Devia, G.K., Ganasri, B.P., Dwarakish, G.S., 2015. A Review on Hydrological Models. Aquat. Procedia 4, 1001–1007. https://doi.org/10.1016/j.aqpro.2015.02.126

FEMA, 2021. https://www.fema.gov/case-study/repetitive-flood-claims-program-benefits-city-and-homeowners [WWW Document].

Field, C., Barros, V., Stocker, T., 2012. Managing the risks of extreme events and disasters to advance climate change adaptation. Special report of the Intergovernmental Panel on Climate Change (IPCC).

Finch, J.W., Bradford, R.B., Hudson, J.A., 2004. The spatial distribution of groundwater flooding in a chalk catchment in southern England. Hydrol. Process. 18, 959–971. https://doi.org/10.1002/hyp.1340

Fish, J.E., Stewart, M.T., 1991. Hydrogeology of the surficial aquifer system, Dade County, Florida, Water-Resources Investigations Report. https://doi.org/10.3133/wri904108

FLO-2D, 2018. FLO-2D Reference Manual.

Franklin, J.L., Avila, L.A., Beven, J.L., Lawrence, M.B., Pasch, R.J., Stewart, S.R., 2001. Atlantic hurricane season of 2000. Mon. Weather Rev. 129, 3037–3056. https://doi.org/10.1175/1520-0493(2001)129<3037:AHSO>2.0.CO;2

Fullerton, W.T., 1983. Water and Sediment Routing from Complex Watersheds and Example Application to Surface Mining. Colorado State University.

García-Gil, A., Vázquez-Suñé, E., Sánchez-Navarro, J.Á., Mateo Lázaro, J., Alcaraz, M., 2015. The propagation of complex flood-induced head wavefronts through a heterogeneous alluvial aquifer and its applicability in groundwater flood risk management. J. Hydrol. 527, 402–419. https://doi.org/10.1016/j.jhydrol.2015.05.005

Gori, A., Lin, N., Smith, J., 2020. Assessing Compound Flooding From Landfalling Tropical Cyclones on the North Carolina Coast. Water Resour. Res. 56. https://doi.org/10.1029/2019WR026788

Greater Miami & the Beaches, 2019. Resilient 305.

Grimaldi, S., Petroselli, A., Arcangeletti, E., Nardi, F., 2013. Flood mapping in ungauged basins using fully continuous hydrologic-hydraulic modeling. J. Hydrol. 487, 39–47. https://doi.org/10.1016/j.jhydrol.2013.02.023

Guha, H., Panday, S., 2012. Impact of Sea Level Rise on Groundwater Salinity in a Coastal Community of South Florida. J. Am. Water Resour. Assoc. 48, 510–529. https://doi.org/10.1111/j.1752-1688.2011.00630.x

Gurdak, J.S., Hanson, R.T., Green, T.R., 2009. Effects of Climate Variability and Change on Groundwater Resources of the United States, Fact Sheet. https://doi.org/10.3133/fs20093074

Harbaugh, A.W., 2005. MODFLOW-2005 : the U.S. Geological Survey modular ground-water model--the ground-water flow process, Techniques and Methods. https://doi.org/10.3133/tm6A16

Hoffmeister, J.E., Stockman, K.W., Multer, H.G., 1967. Miami Limestone of Florida and Its Recent Bahamian Counterpart.

GSA Bull. 78, 175–190. https://doi.org/10.1130/0016-7606(1967)78[175:MLOFAI]2.0.CO;2

Hughes, A.G., Vounaki, T., Peach, D.W., Ireson, A.M., Jackson, C.R., Butler, A.P., Bloomfield, J.P., Finch, J., Wheater, H.S., 2011. Flood risk from groundwater: Examples from a Chalk catchment in southern England. J. Flood Risk Manag. 4, 143–155. https://doi.org/10.1111/j.1753-318X.2011.01095.x

Hughes, J.D., White, J.T., 2016. Hydrologic conditions in urban Miami-Dade County, Florida, and the effect of groundwater pumpage and increased sea level on canal leakage and regional groundwater flow. U.S. Geol. Surv. 175.

Ikeuchi, H., Hirabayashi, Y., Yamazaki, D., Muis, S., Ward, P.J., Winsemius, H.C., Verlaan, M., Kanae, S., 2017. Compound simulation of fluvial floods and storm surges in a global coupled river-coast flood model: Model development and its application to 2007 Cyclone Sidr in Bangladesh. J. Adv. Model. Earth Syst. 9, 1847–1862. https://doi.org/10.1002/2017MS000943

Jacobs, 2007. Groundwater flooding records collation, monitoring and risk assessment (reference HA5): consolidated report.

Jane, R., Cadavid, L., Obeysekera, J., Wahl, T., 2020. Multivariate statistical modelling of the drivers of compound flood events in south Florida. Nat. Hazards Earth Syst. Sci. 20, 2681–2699. https://doi.org/10.5194/nhess-20-2681-2020

Karamouz, M., Zahmatkesh, Z., Goharian, E., Nazif, S., 2015. Combined Impact of Inland and Coastal Floods: Mapping Knowledge Base for Development of Planning Strategies. J. Water Resour. Plan. Manag. 141, 04014098. https://doi.org/10.1061/(asce)wr.1943-5452.0000497

Keenan, J.M., Hill, T., Gumber, A., 2018. Climate gentrification: From theory to empiricism in Miami-Dade County, Florida. Environ. Res. Lett. 13. https://doi.org/10.1088/1748-9326/aabb32

Kumbier, K., Carvalho, R.C., Vafeidis, A.T., Woodroffe, C.D., 2018. Investigating compound flooding in an estuary using hydrodynamic modelling: A case study from the Shoalhaven River, Australia. Nat. Hazards Earth Syst. Sci. 18, 463–477. https://doi.org/10.5194/nhess-18-463-2018

MacDonald, A.M., Lapworth, D.J., Hughes, A.G., Auton, C.A., Maurice, L., Finlayson, A., Gooddy, D.C., 2014. Groundwater, flooding and hydrological functioning in the Findhorn floodplain, Scotland. Hydrol. Res. 45, 755–773. https://doi.org/10.2166/nh.2014.185

Miami-Dade, 2017. Repetitive losses [WWW Document]. URL http://www.miamidade.gov/environment/repetitive-%0Alosses.asp (accessed 9.18.20).

Miami-Dade, 2016. Arch Creek Study Area, Miami-Dade County, Florida; Briefing Book for ULI Advisory Services Panel, May 22-27 2016.

Miami-Dade, 2015. Little Arch Creek Salinity Control Structure; Arch Creek Basin Drainage Evaluation Report.

Miami Herald, 2019. North Miami bought her flooded home. Now it's going to become a park to fight sea rise [WWW Document]. URL https://www.miamiherald.com/news/local/environment/article235403232.html (accessed 10.1.20).

Moftakhari, H., Schubert, J.E., AghaKouchak, A., Matthew, R.A., Sanders, B.F., 2019. Linking statistical and hydrodynamic modeling for compound flood hazard assessment in tidal channels and estuaries. Adv. Water Resour. 128, 28–38. https://doi.org/10.1016/j.advwatres.2019.04.009

Nalesso, M., 2009. Integrated surface-ground water modeling in wetlands with improved methods to simulate vegetative resistance to flow. ProQuest ETD Collect. FIU.

NOAA, 2021. Storm events database [WWW Document]. URL https://www.ncdc.noaa.gov/stormevents/ (accessed 3.29.21).

635 O'Brien, J.S., 2011. FLO-2D Users Manual. Nutrioso, AZ, USA.

O'Brien, J.S., Julien, P.Y., Fullerton, W.T., 1993. Two-dimensional water flood and mudflow simulation. Hydrol. Eng. 244–261.

Ó Dochartaigh, B., Archer, N.A.L., Peskett, L., MacDonald, A.M., Black, A.R., Auton, C.A., Merritt, J.E., Gooddy, D.C., Bonell, M., 2019. Geological structure as a control on floodplain groundwater dynamics. Hydrogeol. J. 27, 703–716. 640 https://doi.org/10.1007/s10040-018-1885-0

Obeysekera, J., Irizarry, M., Park, J., Barnes, J., Dessalegne, T., 2011. Climate change and its implications for water resources management in south Florida. Stoch. Environ. Res. Risk Assess. 25, 495–516. https://doi.org/10.1007/s00477-010-0418-8

Obeysekera, J., Salas, J.D., 2016. Frequency of Recurrent Extremes under Nonstationarity. J. Hydrol. Eng. 21, 04016005. 645 https://doi.org/10.1061/(asce)he.1943-5584.0001339

Obeysekera, J., Sukop, M., Troxler, T., Irizarry, M., Rogers, M., 2019. Potential Implications of Sea-Level Rise and Changing Rainfall for Communities in Florida using Miami-Dade County as a Case Study. Miami FL.

Olbert, A.I., Comer, J., Nash, S., Hartnett, M., 2017. High-resolution multi-scale modelling of coastal flooding due to tides, storm surges and rivers inflows. A Cork City example. Coast. Eng. 121, 278–296. 650 https://doi.org/10.1016/j.coastaleng.2016.12.006

Parker, G.G., Cooke, C.W., 1944. Late Cenozoic Geology of Southern Florida with a Discussion of the Ground Water. U.S. Geol. Surv.

Pellenbarg, N.P., 1989. Groundwater management in the Netherlands: Background and legislation groundwater in the Netherlands. Groundw. Manag. Shar. Responsib. an open access Resour. pp137-149.

655 Peña, F., Nardi, F., 2018. Floodplain terrain analysis for coarse resolution 2D flood modeling. Hydrology 5. https://doi.org/10.3390/hydrology5040052

Peña, F., Nardi, F., Melesse, A., Obeysekera, J., 2021. Assessing geomorphic floodplain models for large scale coarse resolution 2D flood modelling in data scarce regions. Geomorphology 389, 107841. https://doi.org/10.1016/j.geomorph.2021.107841

660 Price, R., Schwartz, K., Anderson, B., Boucek, R., Briceño, H., Cook, M., Fitz, C., Onsted, J., Rehage, J., Rivera-Monroy, V., Roy Chowdhury, R., Saha, A., 2020. Chapter 3: Water, Sustainability, and Survival, in Childers, D.L., E.E. Gaiser and L.A. Ogden (eds.) The Coastal Everglades: The Dynamics of Social-Ecological Transformation in the South Florida Landscape. Oxford University Press : New York, New York.

Prinos, S.T., Dixon, J.F., 2016. Statistical analysis and mapping of water levels in the Biscayne aquifer, water conservation 665 areas, and Everglades National Park, Miami-Dade County, Florida, 2000–2009, Scientific Investigations Report. Reston,

VA. https://doi.org/10.3133/sir20165005

Rotzoll, K., Fletcher, C.H., 2013. Assessment of groundwater inundation as a consequence of sea-level rise. Nat. Clim. Chang. 3, 477–481. https://doi.org/10.1038/nclimate1725

Saksena, S., Merwade, V., Singhofen, P.J., 2019. Flood inundation modeling and mapping by integrating surface and subsurface hydrology with river hydrodynamics. J. Hydrol. 575, 1155–1177. https://doi.org/10.1016/j.jhydrol.2019.06.024

Santiago-Collazo, F.L., Bilskie, M. V., Hagen, S.C., 2019. A comprehensive review of compound inundation models in low-gradient coastal watersheds. Environ. Model. Softw. 119, 166–181. https://doi.org/10.1016/j.envsoft.2019.06.002

Sebastian, A., Dupuits, E.J.C., Morales-Nápoles, O., 2017. Applying a Bayesian network based on Gaussian copulas to model the hydraulic boundary conditions for hurricane flood risk analysis in a coastal watershed. Coast. Eng. 125, 42–50. https://doi.org/10.1016/j.coastaleng.2017.03.008

Seneviratne, S., Nicholls, N., Easterling, D., Goodess, C., Kanae, S., Kossin, J., Luo, Y., Marengo, J., Mcinnes, K., Rahimi, M., Reichstein, M., Sorteberg, A., Vera, C., Zhang, X., 2012. Changes in climate extremes and their impacts on the natural physical environment.

Sepúlveda, N., 2021. Evaluation of actual evapotranspiration rates from the Operational Simplified Surface Energy Balance (SSEBop) model in Florida and parts of Alabama and Georgia, 2000–17, Scientific Investigations Report. Reston, VA. https://doi.org/10.3133/sir20215072

Serafin, K., Ruggiero, P., Parker, K., Hill, D., 2019. What's streamflow got to do with it? A probabilistic simulation of the competing oceanographic and fluvial processes driving extreme along-river water levels. Nat. Hazards Earth Syst. Sci. 1–30. https://doi.org/10.5194/nhess-2018-347

SFWMD, 2021. DBHYDRO [WWW Document]. URL http://my.sfwmd.gov/dbhydroplsql/show_dbkey_info.main_menu (accessed 1.1.21).

Singh, S.P., Azua, A., Chaudhary, A., Khan, S., Willett, K.L., Gardinali, P.R., 2010. Occurrence and distribution of steroids, hormones and selected pharmaceuticals in South Florida coastal environments. Ecotoxicology 19, 338–350. https://doi.org/10.1007/s10646-009-0416-0

Smith, M.A., Kominoski, J.S., Gaiser, E.E., Price, R.M., Troxler, T.G., 2021. Stormwater runoff and tidal flooding transform dissolved organic matter composition and increase bioavailability in urban coastal ecosystems. J. Geophys. Res. Biogeosciences 1–19. https://doi.org/10.1029/2020jg006146

Sophocleous, M., 2002. Interactions between groundwater and surface water: The state of the science. Hydrogeol. J. 10, 52–67. https://doi.org/10.1007/s10040-001-0170-8

Southeast Florida Regional Climate Change Compact Sea Level Rise Work Group (Compact), 2020. A document prepared for the Southeast Florida Regional Climate Change Compact Climate Leadership Committee.

Su, X., Liu, T., Beheshti, M., Prigiobbe, V., 2020. Relationship between infiltration, sewer rehabilitation, and groundwater flooding in coastal urban areas. Environ. Sci. Pollut. Res. 27, 14288–14298. https://doi.org/10.1007/s11356-019-06513-

700 z

Sukop, M.C., Rogers, M., Guannel, G., Infanti, J.M., Hagemann, K., 2018. High temporal resolution modeling of the impact of rain, tides, and sea level rise on water table flooding in the Arch Creek basin, Miami-Dade County Florida USA. Sci. Total Environ. 616–617, 1668–1688. https://doi.org/10.1016/j.scitotenv.2017.10.170

Sweet, W. V., Menendez, M., Genz, A., Obeysekera, J., Park, J., Marra, J.J., 2016. In tide's way: Southeast Florida's September
705   2015 sunny-day flood. Bull. Am. Meteorol. Soc. 97, S25–S30. https://doi.org/10.1175/BAMS-D-16-0117.1

Taylor, C.J., Alley, W.M., 2001. Ground-water-level monitoring and the importance of long-term water-level data. US Geol. Surv. Circ. 1–68.

Teng, J., Jakeman, A.J., Vaze, J., Croke, B.F.W., Dutta, D., Kim, S., 2017. Flood inundation modelling: A review of methods, recent advances and uncertainty analysis. Environ. Model. Softw. 90, 201–216.
710   https://doi.org/10.1016/j.envsoft.2017.01.006

U.S. Census Bureau, 2020. American Community Survey 5-Year Data (2009-2019) [WWW Document]. URL https://www.census.gov/data/developers/data-sets/acs-5year.html (accessed 7.18.21).

U.S. Department of Agriculture, 1948. Aerial photographs of Dade County [WWW Document]. URL https://ufdc.ufl.edu/UF00071738/00034/1x?search=dade

715 van Westen, C.J., Greiving, S., 2017. Multi-hazard risk assessment and decision making. Environ. Hazards Methodol. Risk Assess. Manag. 31–94. https://doi.org/10.2166/9781780407135_0031

Wahl, T., Jain, S., Bender, J., Meyers, S.D., Luther, M.E., 2015. Increasing risk of compound flooding from storm surge and rainfall for major US cities. Nat. Clim. Chang. 5, 1093–1097. https://doi.org/10.1038/nclimate2736

Wdowinski, S., 2019. Coherent saptio-temporal variations in the rate of sea level rise along the US Atlantic and Gulf coasts,
720   in: AGU Fall Meeting Abstracts. pp. OS21A-07.

Winston, R.B., 2009. ModelMuse: A Graphical User Interface for MODFLOW-2005 and PHAST: U.S. Geological Survey Techniques and Methods 6–A29.

Yang, S., Tsai, F.T.C., 2020. Understanding impacts of groundwater dynamics on flooding and levees in Greater New Orleans. J. Hydrol. Reg. Stud. 32, 100740. https://doi.org/10.1016/j.ejrh.2020.100740

725 Yang, Y., Toor, G., Wilson, P.C., Williams, C.F., 2016. Septic systems as hot-spots of pollutants in the environment: Fate and mass balance of micropollutants in septic drainfields. Sci. Total Environ. 566–567, 1535–1544.

Yu, X., Moraetis, D., Nikolaidis, N.P., Li, B., Duffy, C., Liu, B., 2019. A coupled surface-subsurface hydrologic model to assess groundwater flood risk spatially and temporally. Environ. Model. Softw. 114, 129–139. https://doi.org/10.1016/j.envsoft.2019.01.008

730 Zhang, K., Li, Y., Liu, H., Xu, H., Shen, J., 2013. Comparison of three methods for estimating the sea level rise effect on storm surge flooding. Clim. Change 118, 487–500. https://doi.org/10.1007/s10584-012-0645-8

Zscheischler, J., Westra, S., Van Den Hurk, B.J.J.M., Seneviratne, S.I., Ward, P.J., Pitman, A., Aghakouchak, A., Bresch, D.N., Leonard, M., Wahl, T., Zhang, X., 2018. Future climate risk from compound events. Nat. Clim. Chang. 8, 469–

477. https://doi.org/10.1038/s41558-018-0156-3

735
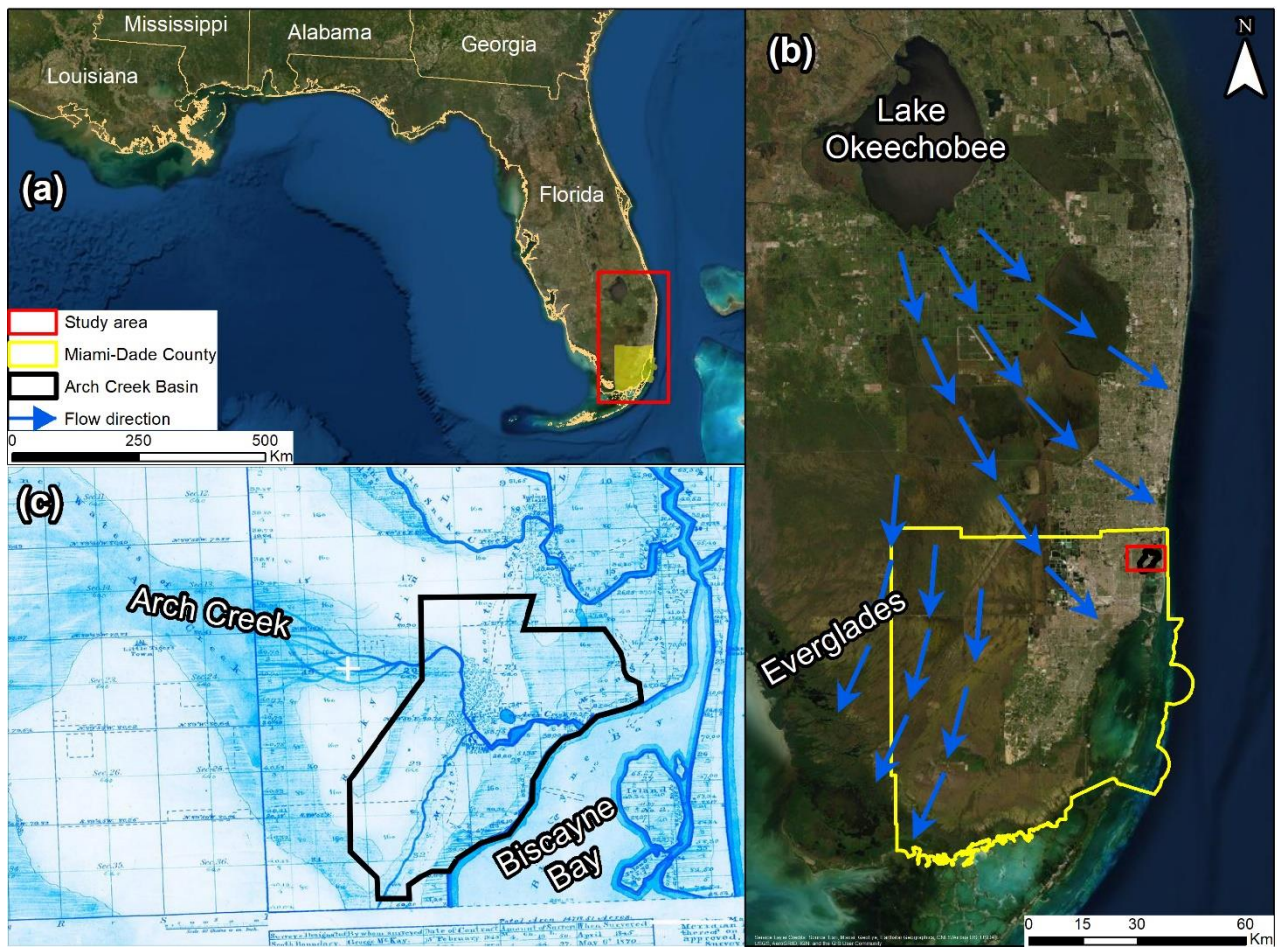
Figure 1. Location map of the study area. (a) MDC located in Southeast Florida, USA (b) current Everglades water flow from Lake Okeechobee towards the Atlantic Coast and Gulf of Mexico, and (c) land survey from 1870 that illustrates the natural flow direction of the Arch Creek to discharge into the Biscayne Bay prior urbanization (Miami Herald, 2019).
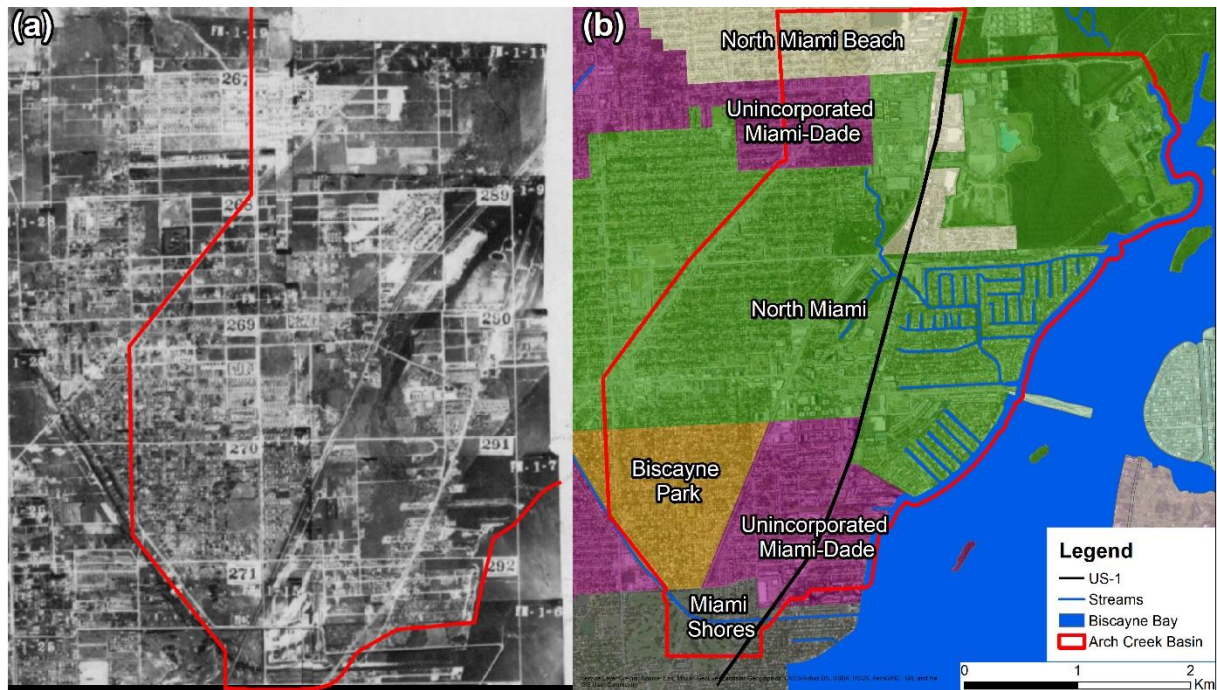
Figure 2. Aerial photography that compares historical (1948) and current urbanized environment in the study area. (a) Major civil and drainage works contributed to the rapid urbanization of the Arch Creek Basin; (b) Municipality map, including North Miami, Biscayne Park, North Miami Beach, Miami Shores and Unincorporated Miami-Dade (U.S. Department of Agriculture, 1948).

Table 1. Population and land elevations of Arch Creek Basin jurisdictions. Population totals account for the whole jurisdiction area (U.S. Census Bureau, 2020)

Jurisdiction	Population*	Area (km²)	Area ACB (km²)	Percentage of land elevation (meters)				
				< 0	0 - 1	1 - 2	2 - 5	> 5
North Miami	62489	26.09	11.00	7.88	18.64	39.67	31.27	2.54
Biscayne Park	3124	1.64	1.44	0.00	1.48	77.20	21.32	0.00
North Miami Beach	42971	13.79	1.43	0.01	11.53	20.05	68.41	0.00
Miami Shores	10459	9.80	0.54	4.82	19.68	38.91	36.56	0.03
Unincorporated MDC	N/A	25467	2.54	3.65	14.60	47.08	34.67	0.00

750
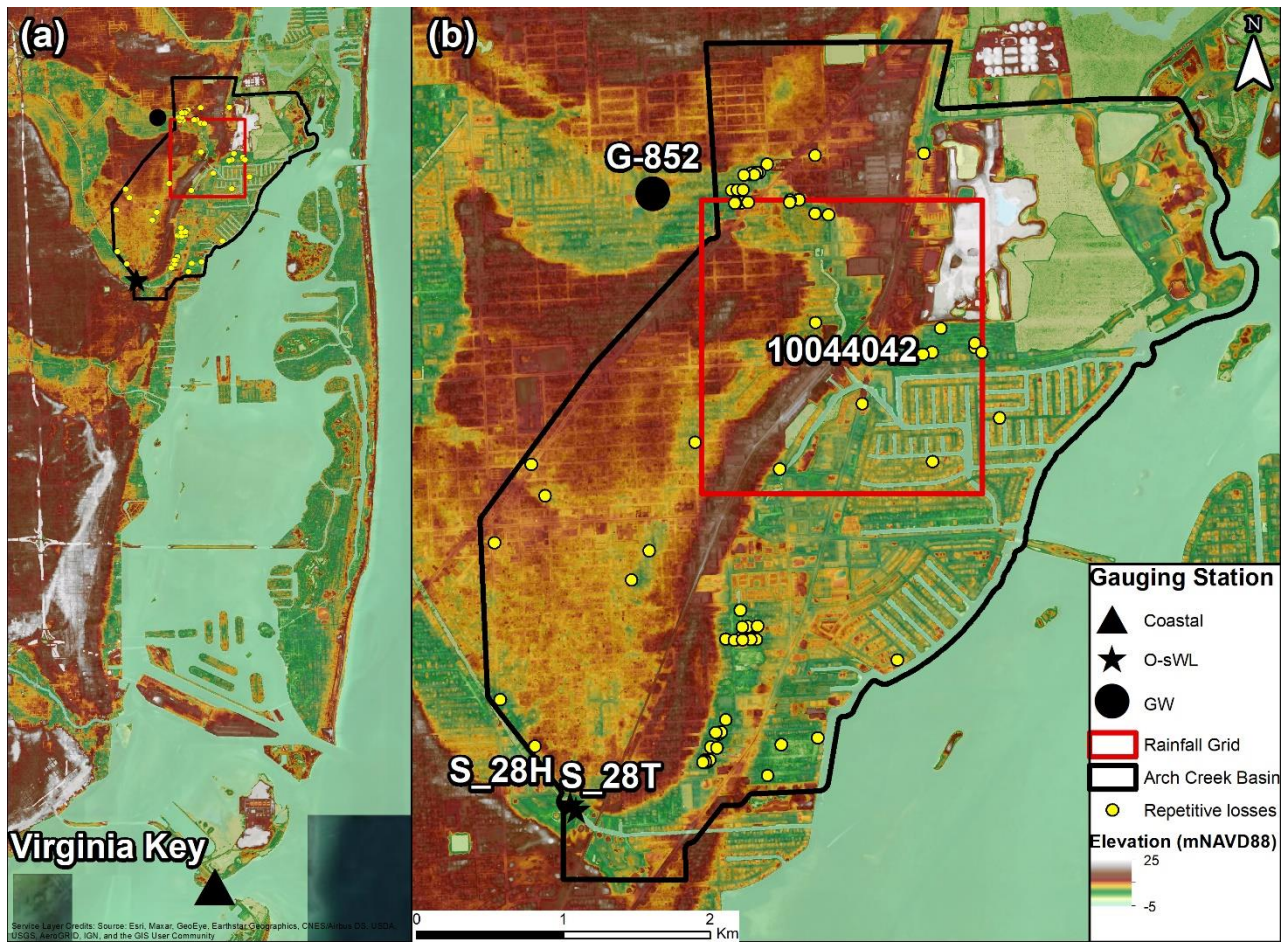
Figure 3. Geographical location of selected data in the study site. (a-b) Topographic map showing the location of the Arch Creek Basin (black polygon), and the distribution of closest gauging stations to the study site (black markers), rainfall grid (red square), and properties
755   that have experience severe repetitive losses due to flooding events (yellow).
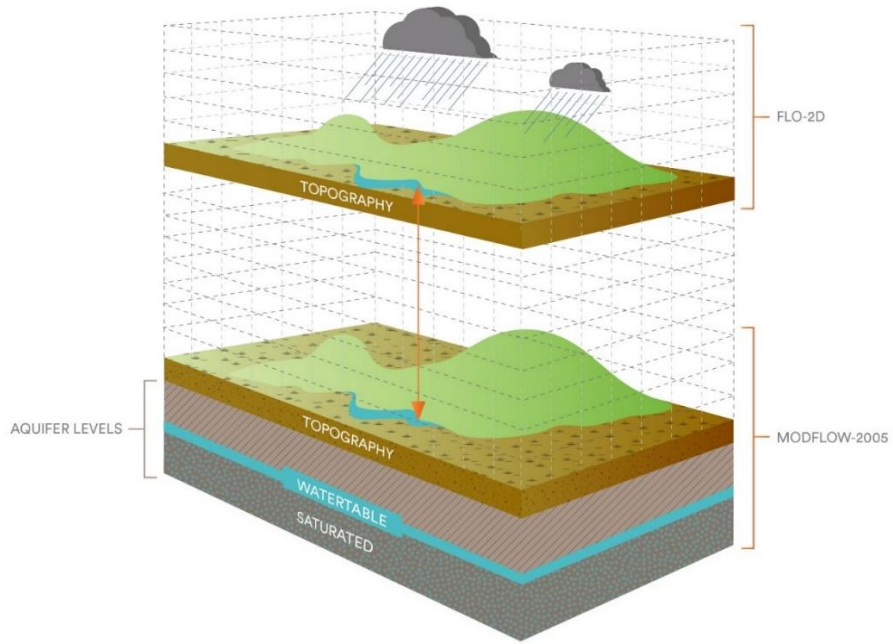
Figure 4. Spatial compatibility between FLO-2D and MODFLOW-2005.

760
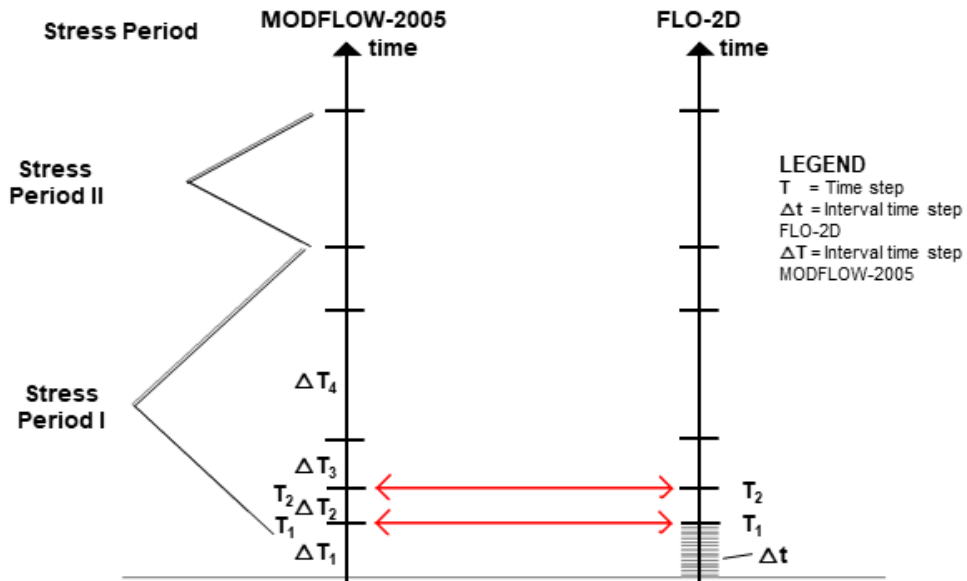
Figure 5. Time-step synchronization of FLO-2D and MODFLOW-2005.
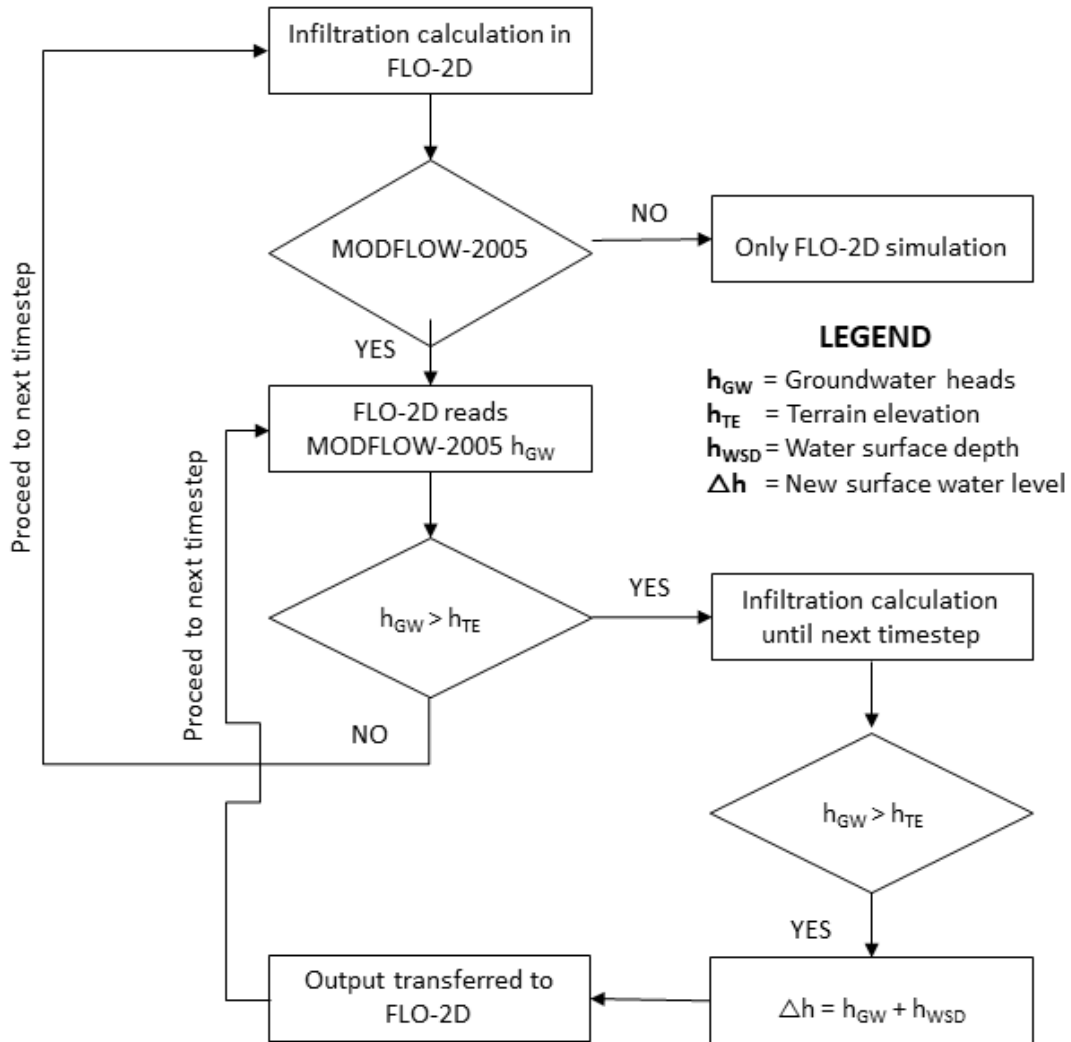
765

Figure 6. Conceptual diagram of the infiltration methodology incorporated in the coupled FLO-2D and MODFLOW-2005 that illustrates the influence of groundwater heads in the infiltration calculation. Adapted from (Nalesso, 2009)**.**
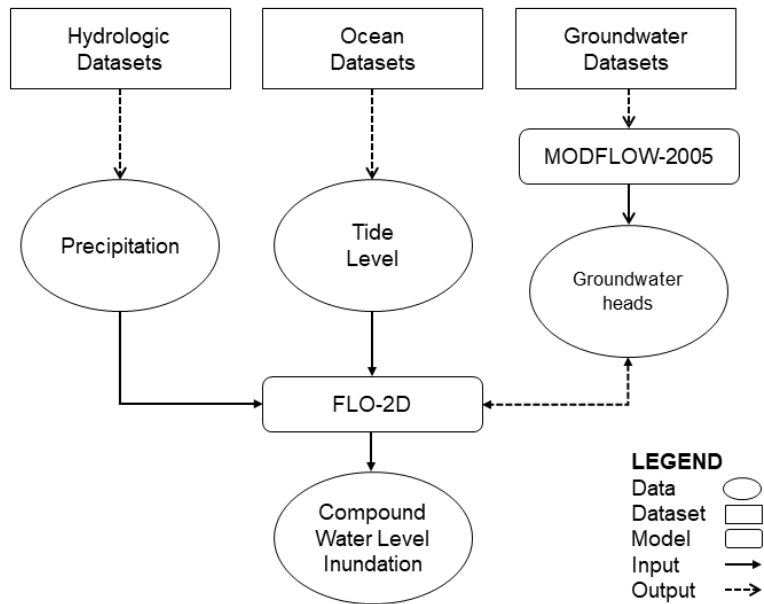
770

Figure 7. Flowchart representing the CF simulation using FLO-2D as the base hydraulic model. The hydrologic, ocean, and groundwater datasets were obtained through observations. The surface hydrology was incorporated as rainfall and coastal boundary conditions in FLO-2D. The groundwater heads were calculated in MODFLOW-2005 and transferred in an iterative manner to FLO-2D every time a MODFLOW-2005 time step is reached (Fig. 6). Adapted from Santiago-Collazo et al. (2019)
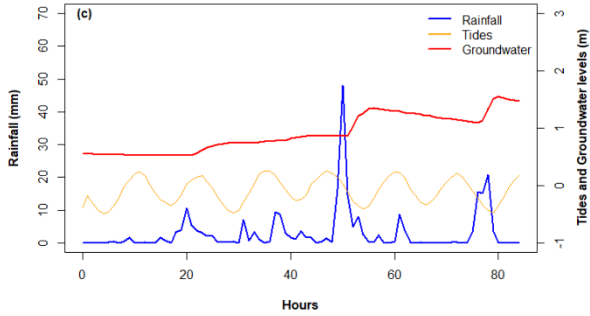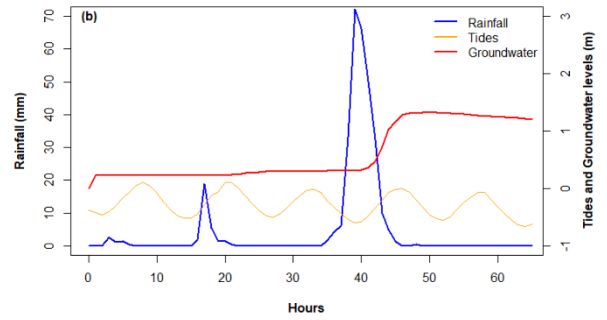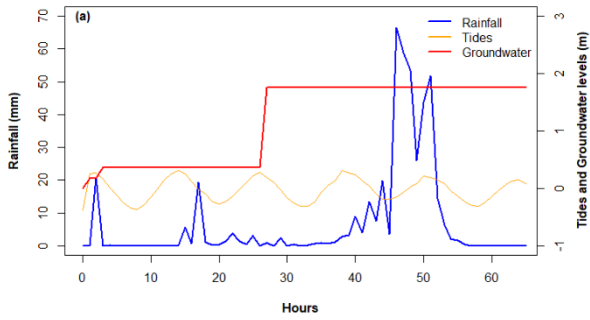
Figure 8. Time series of rainfall, tides, and groundwater levels for: (a) Tropical Storm Leslie; (b) Tropical Storm Andrea; (c) 25 May 2020 storm. The simulation time was determined based on the rainfall duration and groundwater fluctuations to properly characterized each event, being 64-hours for both Tropical Storms and 84-hours for the May 2020 event.

Service Layer Credits: Source: Esri, Maxar, GeoEye, Earthstar Geographics, CNES/Airbus DS, USDA, USGS, AeroGRID, IGN, and the GIS User Community
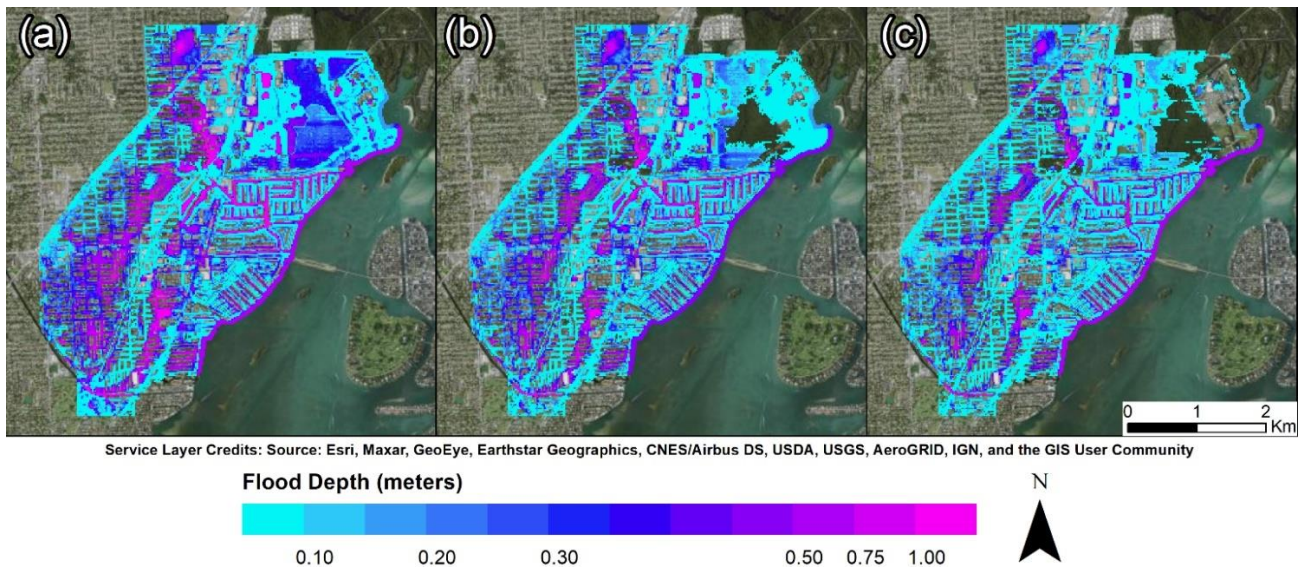
Figure 9. Spatial distribution of maximum inundation depths for Tropical Storm Leslie (a), Tropical Storm Andrea (b), and 25 May 2020 event (c).

Service Layer Credits: Source: Esri, Maxar, GeoEye, Earthstar Geographics, CNES/Airbus DS, USDA, USGS, AeroGRID, IGN, and the GIS User Community
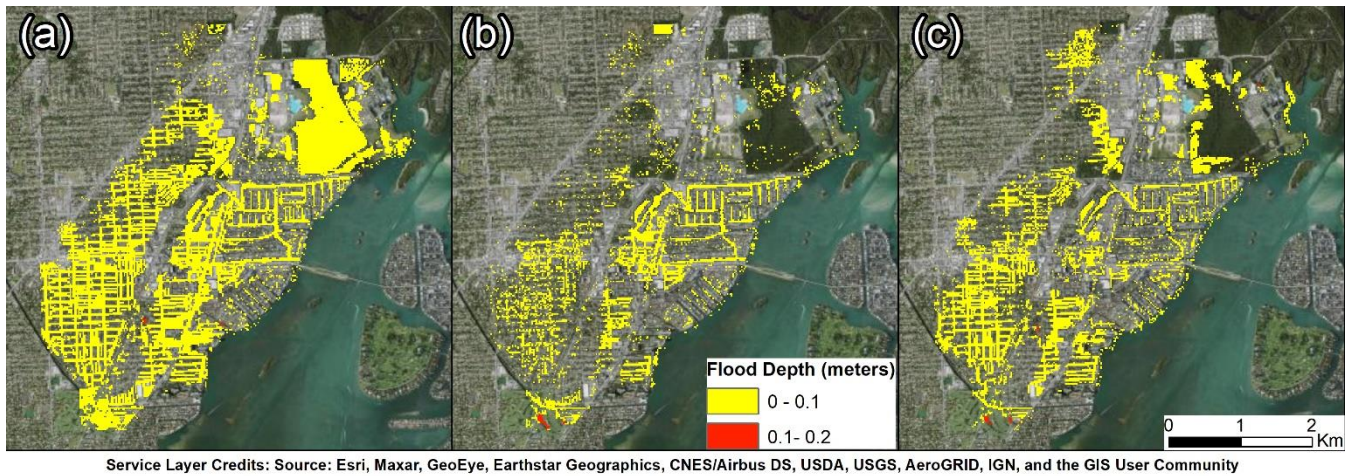
Figure 10. Spatial distribution of groundwater-induced flooding for Tropical Storm Leslie (a), Tropical Storm Andrea (b), and 25 May 2020 event (c).

790
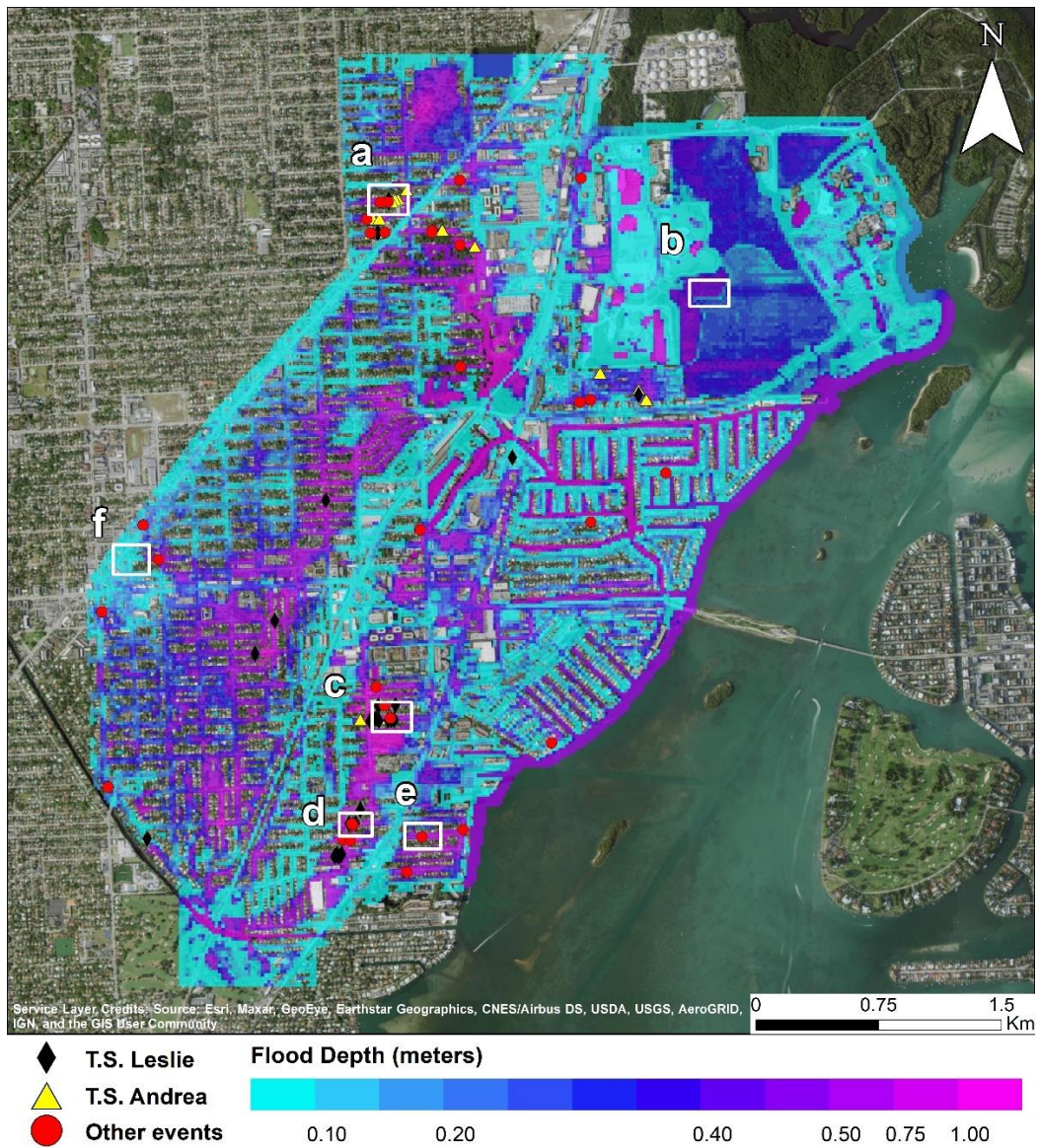
Figure 11. Distribution of maximum flood depths for Tropical Storm Leslie. The markers indicate repetitive loss properties caused by Tropical Storm Leslie (black), Tropical Storm Andrea (yellow) or other storm events (red). Maximum flood depths at six sample locations (white) are presented in Fig. 11.
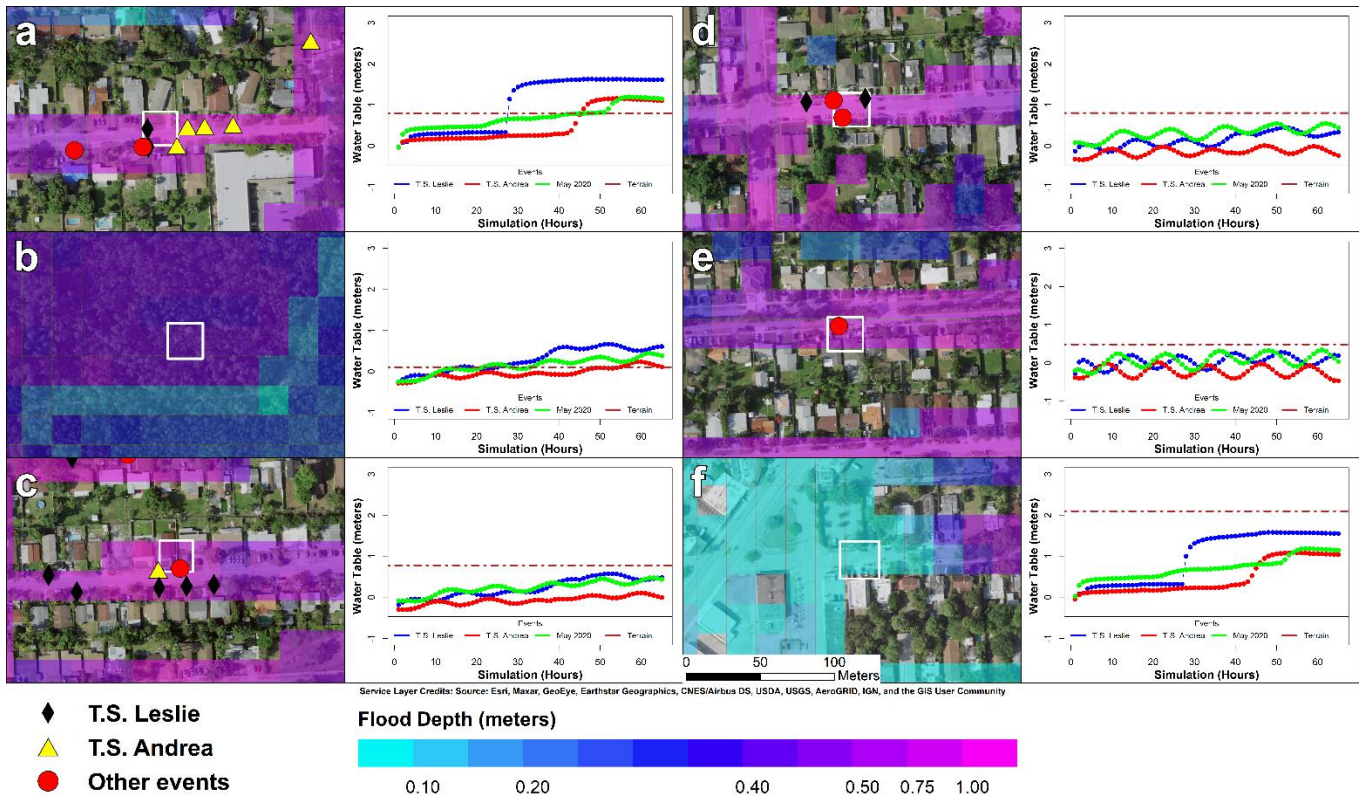
Figure 12. Six sample locations (Fig. 10) are selected to observe the maximum flood depths for Tropical Storm Leslie (left). The markers display repetitive loss properties that have been affected by Tropical Storm Leslie (black), Tropical Storm Andrea (yellow), and other storm events (red). The water table timeseries (left) display the behavior of the groundwater heads during Tropical Storm Leslie (blue line), Tropical Storm Andrea (red line) and the 25 May 2020 event (green line) at a specific location (white). Results demonstrate that the simulated water table (right pane) exceeded the surface elevation (brown line) on two locations leading to groundwater-induced flooding (a-b) while the rest are driven by pluvial flooding (c-d-e-f).

Table 2. Quantitative analysis of simulated flood depths in respect to FEMA's repetitive loss properties database by events.

Flood depth (mts)	T.S. Leslie	T.S. Andrea	Other Events
0 - 0.1	2	0	3
0.1 - 0.2	1	1	5
0.2 - 0.3	0	1	3
0.3 - 0.4	1	1	5
0.4 - 0.5	0	2	5
0.5 - 0.75	4	5	10
0.75 - 1.0	13	7	2
1.0 - 2.0	4	0	0
Total	25	17	33

Table 3. Comparison between simulated maximum water flood depths and VGI imagery obtained during and after Tropical Storm Andrea.

No.	Latitude	Longitude	Image category	Interpreted depth (m)	Max simulated depth (m)	Difference (m)
1	-80.165579	25.910225	During storm	0.20	0.67	-0.47
2	-80.157365	25.908227	During storm	0.55	0.54	0.01
3	-80.170807	25.900715	After storm	0.25	0.23	0.02

810

815
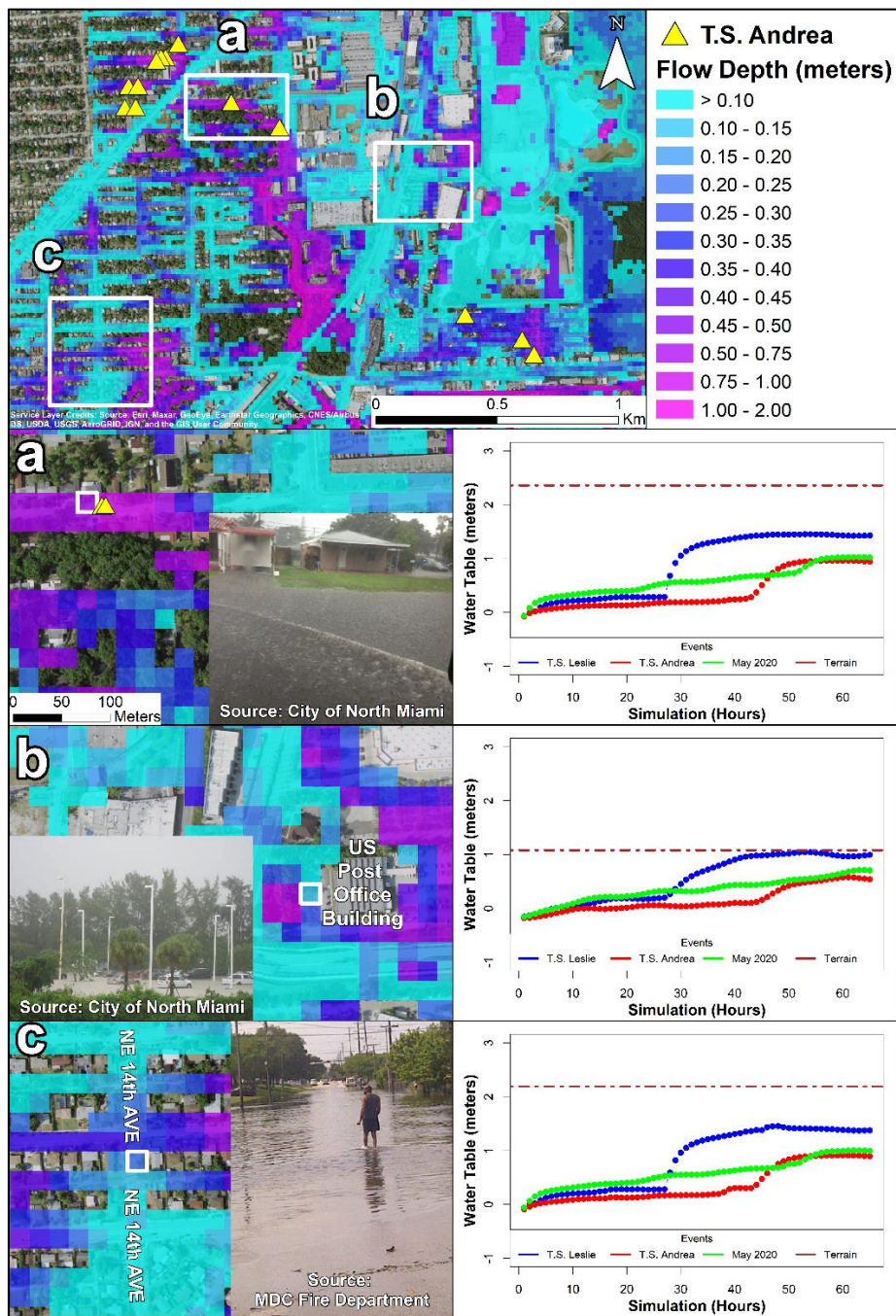
Figure 13. Maximum flood depths for Tropical Storm Andrea in the Northwestern portion of the Arch Creek Basin (top). The marker (yellow) display properties that were affected during Tropical Storm Andrea. Three sample locations (white) are presented as subdomains (a-b-c) and available crowdsourced observations display the flooding conditions at a specific cell (white). The simulated water table timeseries (right pane) show that groundwater heads remained below the surface elevation (brown line); thus, all three locations experienced rainfall-induced flooding.